Engineering Structures 138 (2017) 410–424

Contents lists available at ScienceDirect

Engineering Structures

journal homepage: www.elsevier.com/locate/engstruct

Nonlinear dynamic numerical analysis of a RC frame subjected to seismic loading

Martín Domizio, Daniel Ambrosini *, Oscar Curadelli

Structural Engineering Master Program, National University of Cuyo, Mendoza, Argentina
CONICET, National Research Council, Argentina

ARTICLE INFO

Article history:
Received 2 April 2016
Revised 10 February 2017
Accepted 11 February 2017

Keywords:
Non-linear dynamic analysis
Concrete material model
Numerical model calibration
Numerical-experimental comparison

ABSTRACT

In the context of seismic engineering, reliable modeling methodologies are needed to represent the non-linear dynamic behavior of structures under the effect of the seismic action. Only in this way is it possible to assess the safety margin against structural collapse. However, in the case of reinforced concrete (RC) structures, numerical modeling still presents difficulties due to complex nonlinear material behavior. The aim of this paper is to evaluate the capability of numerical modeling with solid finite elements to represent a strongly nonlinear dynamic response of reinforced concrete structures under the effect of the seismic action. A second objective is to obtain modeling guidelines for this dynamic behavior. A numerical study was performed in order to reproduce the nonlinear dynamic response of a RC frame tested by Elwood and Moehle (2003) on a shaking table at the University of California, Berkeley (USA). A material model that employs the shear failure surface proposed by Ottosen (1977) was selected to represent the non-linear behavior of concrete. This material model has several parameters that define their behavior, which includes the crack width at which tensile stress decreases to zero after a strain softening process. This parameter and the strain based erosion limit were subjected to calibration. During the calibration process, the degree of numerical-experimental similarity was established along with conclusions about the sensitivity of numerical response to variations of the calibrated parameters. Finally, it can be concluded that the numerical model reproduces the nonlinear response with sufficient accuracy. Moreover, the explicit time integration scheme shown to be appropriate for this type of problem with strong nonlinearities and degradation of the concrete.

1. Introduction

The main objective of seismic engineering is to reduce the structural vulnerability against seismic action. In order to achieve this goal, it is necessary to establish the safety margin against structural collapse using models that are able to accurately and reliably predict the nonlinear dynamic behavior of structures. In the particular case of RC structures, the modeling of nonlinear behavior is highly complex, being subject of a field of research that continuously makes developments and innovations on this topic.

In order to model the nonlinear behavior of RC structures, multiple approaches that apply the finite element method have been formulated. The use of lumped plasticity models represents the simplest way to reproduce this nonlinear behavior. Such models are computationally efficient and stable, being studied at present by several authors [3–8]. A lumped plasticity model represented by a plastic hinge that takes into account axial–shear–flexure interaction was proposed by Xu and Zhang [9]. The authors show that the proposed model is able to reproduce degradation, softening and pinching of reinforced concrete columns against the seismic action. A dual plastic hinge that combines the nonlinear flexural response of beams with the nonlinear behavior of joints in RC frames was proposed by Birely et al. [10]. Hinge parameters were calibrated with experimental results, showing a good agreement in terms of stiffness, strength and drift capacity. Beyond the advantages of this type of modeling, it is important to take into account that its use may be limited due to excessive simplifications.

Other kinds of elements, currently used in practice and research, are those employing a distributed plasticity approach, such as fiber elements. In these models, the cross-section forces are obtained from stress integration over each fiber. In turn, these stresses are obtained from a constitutive relationship and a pre-established deformation hypothesis. Like lumped plasticity mod-

* Corresponding author at: Facultad de Ingeniería, Centro Universitario, Parque Gral. San Martín, (5500) Mendoza, Argentina.
E-mail address: dambrosini@uncu.edu.ar (D. Ambrosini).

http://dx.doi.org/10.1016/j.engstruct.2017.02.031
0141-0296/

els, the fiber elements are also efficient in terms of computational cost, but they can solve more general problems, being studied currently by several authors [11–18]. Martinelli et al. [19] analyzed the capability of fiber elements to reproduce the experimental response of a 5 story lightly reinforced shear wall, which was tested on a shaking table. In this study, a type of displacement-based element that takes into account the shear-flexure interaction was proposed, showing a good correlation with experimental response. The fiber element proposed by Lobo and Almeida [20] takes into account the possibility of slip of the steel reinforcement in concrete. This force-based fiber element proves to be able to precisely reproduce the experimental behavior of beam–column subassemblage with reduced anchorage length subjected to cyclic loading. Leborgne and Ghannoum [21] propose a new fiber element able to simulate cyclic degradation and damage of lightly confined RC columns that reach flexural yielding before shear failure resulting from strength degradation. Expressions that define cyclic behavior directly from geometric and material properties of the columns were established through regression analysis and a parameter calibration process. Caprili et al. [22] used force-based fiber elements to assess the seismic vulnerability of a 5-story RC building constructed in the early 1960s. The authors calibrated the numerical model with experimental results and compared the results obtained with different analysis methods. The use of these distributed plasticity models is limited to those cases where the cross-section deformation assumptions can be verified and where the structural element can be represented by its longitudinal axis.

The triaxial stress and strain states in RC structures caused by seismic action can be obtained directly from solid finite element models, as a function of the nonlinear material constitutive laws adopted. Due to this, the use of solid finite elements represents the most general and direct method to simulate the dynamic response of structures. It should be mentioned that a relatively large amount of elements is needed to represent the nonlinear behavior of structures correctly, which is very expensive in terms of computational resources and time. In order to reduce the computational effort, solids elements can be used only in critical parts of the structure and can be combined with less refined elements to represent the rest of the structure. Moreover, the attempt to simulate the dynamic response of RC structures using an implicit time integration scheme can lead to convergence problems. This results from the strongly nonlinear dynamic behavior of RC structures that suffers strength and stiffness degradation against seismic action. Because of this, an explicit integration scheme was adopted in this paper to simulate the response of RC structures, using a solid finite element model developed with LS-DYNA [23] software. There are numerous precedents on the use of these types of models in the study of the behavior of RC structures against blast loads [24–28] and impact loads [29–33], but it is less common to use these models when analyzing the structural response under seismic action.

The calibration and validation of numerical models against experimental results is essential for obtaining reliable predictions about the nonlinear dynamic response of RC structures, regardless of the modeling methodology employed. Therefore, the contribution of this paper is to quantify the degree of experimental-numerical correlation that can be achieved using a solid finite element model to reproduce the damage of a RC structure under the effect of the seismic action. A second objective is to obtain modeling guidelines for this phenomenon, which could be used by other researchers and engineers.

In this paper a numerical study was performed in order to reproduce the nonlinear dynamic response of a RC frame tested by Elwood and Moehle [1] on a shaking table at the University of California, Berkeley (USA). In order to represent the behavior of the concrete, a material model capable of reproducing concrete cracking and crushing was adopted. This material model uses the shear failure surface proposed by Ottosen [2]. Two parameters that define the behavior of the model were calibrated in this study: the first calibrated parameter is the opening width of the crack from which the normal stress crack decreases to zero; and, the second is the limit erosion value from which the elements are removed from the numerical model. Two different strain based erosion criteria were evaluated. Sensitivity of the numerical response to the variation of these parameters was analyzed, along with the degree of similarity to the experimental response that can be achieved by the numerical model.

2. Experimental program

A series of dynamic tests were performed by Elwood and Moehle [1,34] in order to study the behavior of RC frame columns with low transverse reinforcement. Such columns are vulnerable to shear failure, and are still present in structures designed with building codes prior to the 1970s. Experimental tests were performed on a shaking table at the Earthquake Engineering Research Center at the University of California, Berkeley, simulating the effect of the seismic action in the plane direction of the frame. The RC frames tested had three columns, with steel reinforcing bars disposed as shown in Fig. 1.

The center column represents, in half-scale, the column studied by Lynn [35] and Sezen [36], with a weak transverse reinforcement consisting of 4.9 mm diameter ties spaced at 152 mm. This column was designed to reach the yielding of the longitudinal reinforcement first, with a subsequent loss of axial load capacity and shear strength. The outer columns were designed to support the redistribution of the axial load and shear force due to degradation of the center column induced by the seismic action. These columns had a circular cross section and a spiral transverse reinforcement with 9.5 mm diameter and 5.08 cm spacing, allowing them to develop a ductile behavior. Furthermore, beams that connect the three columns, and their respective foundations were designed by capacity. A total mass of 31000 kg was achieved adding lead packages on the beams. Two identical specimens were built, applying an extra axial load by pneumatic actuators, on the center column of the second specimen. The axial load on the center column in the first test represented 10% of the nominal axial column strength, while in the second test reached 24%. In this paper, the dynamic response of the first tested specimen was used as reference in the numerical model calibration.

A series of tests was performed in order to determine the properties of the materials used in the construction of the specimens. Results from three concrete cylinders representative of specimen 1 are summarized in Table 1, and results of tests on reinforcing bars are summarized in Table 2.

The experimental model was fully instrumented to record their dynamic response. In order to record the three-dimensional movement of the shaking table 8 displacement sensors and 8 accelerometers were used. A pair of force transducers was placed under each column to measure shear and moment. The displacements of the specimen were measured with respect to the shaking table and with respect to an external frame using linear variable differential transformers (LVDT). The accelerations of the specimen were also recorded, as well as the local deformations of the center column using direct current displacement transducers (DCDT) and strains in the reinforcement bars using strain gauge. In particular, the experimental data of the displacement measured in the upper end of the center column relative to its foundation, the base shear measured by load cells in this center column, and the acceleration recorded on the shaking table were used in the calibration of the numerical model.

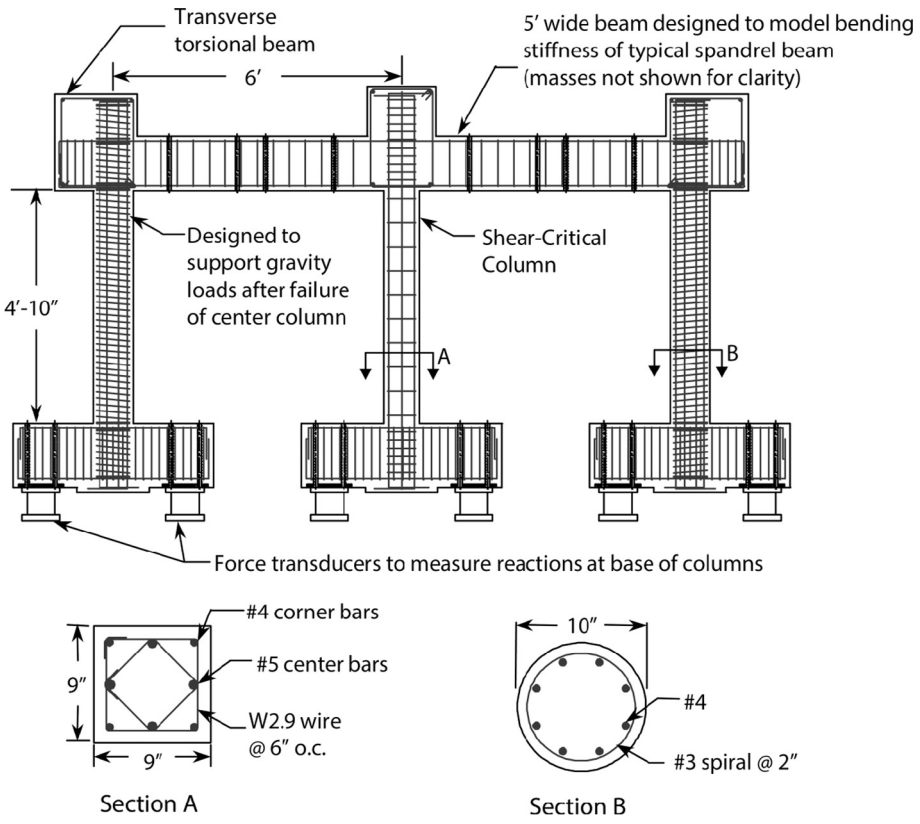

Fig. 1. Steel reinforcement of the experimental model [1].

Table 1
Test results of concrete specimens (extracted from [1]).

Structural Element	Age (days)	Compressive strength (MPa)			Tensile strength (MPa)
		Mean Value	Min. Value	Max. Value	Mean Value
Beams and Columns	165	24.54	24.07	25.11	2.48
Foundation	221	22.34	21.52	23.63	2.32

Table 2
Test results of steel specimens (extracted from [1]).

Element	Reinforcement	Diameter (cm)	Yield Stress (MPa)	Ultimate Stress (MPa)	Yield Strain	Ultimate Strain	Elastic Modulus (GPa)
Center Column	Long.	1.27/1.59	479.1	689.4	0.0027	0.2020	199.5
	Trans.	0.49	–	717.0	–	0.0220	204.0
External Column	Long	1.27	424.0	654.9	0.0024	0.2040	199.6
	Trans.	0.95	547.4	723.9	0.0028	0.1380	201.6
Beam	Long	0.95/1.27	547.4	723.9	0.0028	0.1380	201.6
	Trans.	0.95	547.4	723.9	0.0028	0.1380	201.6

The experimental program consisted of free vibrations and forced vibrations tests. A horizontal component of the ground motion registered in Viña del Mar during the 1985 earthquake was used in the forced vibrations test. This seismic record was selected to induce a response level with sufficient amplitude to observe the failure in the center column without reaching the maximum ductility demand in the outer columns. The acceleration recorded at shaking table during destructive seismic test of specimen 1 is shown in Fig. 2, and the corresponding response spectrum, taking into account an inherent damping of 2%, is shown in Fig. 3.

The original record was used with two amplitude levels in each specimen. First, a dynamic test with a scale factor of 0.13 was made in order to observe the dynamic response of the structure without reaching the level of displacement needed to start yielding in the center column. Later, a forced vibration test with scale factor 1 was performed, reaching the failure in the center column. Free vibration tests were performed before and after each test with seismic records. A fundamental period of 0.22 s and 1.9% of damping ratio were measured before forced vibrations tests. After the forced vibration test where degradation in the center column was observed, a fundamental period of 0.68 s and 5.4% damping were measured.

From the results of forced vibrations test, it was observed that an increase of the axial load in the second specimen produced an earlier shear failure in the center column, as well as a greater loss

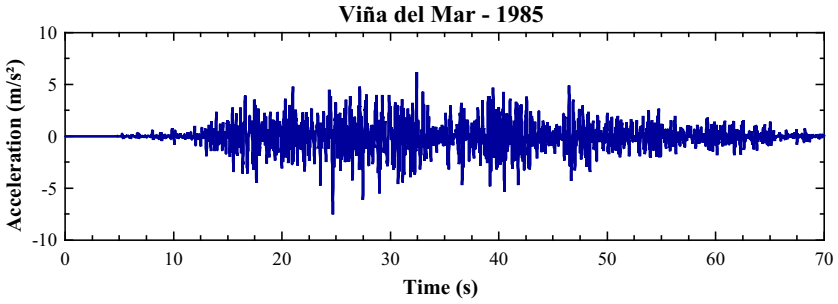

Fig. 2. Acceleration time history of Viña del Mar (Chile, 1985) seismic record.

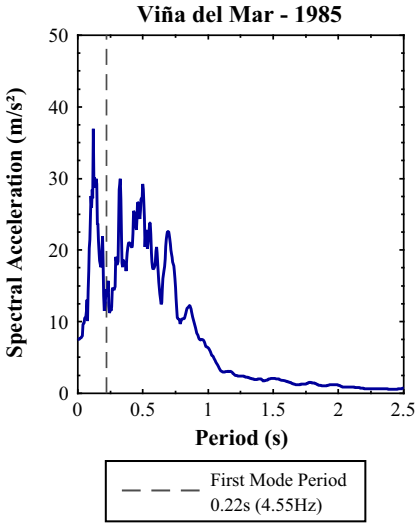

Fig. 3. Response spectrum of Viña del Mar (Chile, 1985) seismic record.

in axial load capacity, further redistributing forces to external columns. The onset of loss of axial load capacity in the center column of the second specimen was coincident with the largest increase in horizontal displacement, after that the axial load capacity continued to decrease more slowly with lower displacements during several cycles of oscillation, indicating a process of gradual degradation. A dynamic amplification was also observed in the redistribution of axial load, resulting from the vertical oscillations of the beam. In both specimens, stiffness and shear strength of the center column became virtually zero after the first 30 s of the seismic record, observing a residual lateral displacement after this instant of time.

3. Description of the numerical model

The numerical model of the analyzed structure was developed using LS-DYNA [23] software. Hexahedral solid elements with constant stress and one integration point were used for modeling concrete. Since this type of elements are under-integrated, a stabilization method was necessary to control spurious deformation modes without associated energy, known as Hourglass modes. For this purpose, Flanagan-Belytschko stabilization [23,37], proportional to the stiffness with exact volume integration, was used. Meanwhile, the longitudinal and transverse steel reinforcement was modeled with Hughes-Liu beam elements [23,38,39], with cross section integration.

The solid finite elements representing the concrete and the beam finite elements representing the steel reinforcement shared the same nodes, thereby establishing the transfer of stresses and strain compatibility between them. This method assumes a perfect bond between steel and concrete, and is not able to represent slip of steel bars embedded in the concrete, which could be important if anchorage length is insufficient or if the structural element is subjected to several cycles where bond stress exceeds 80% of the maximum bond resistance [40,41]. On the other hand, if the anchorage is properly designed and built, slippage is minimum and the hypothesis of perfect bond is reasonable. In the case of the analyzed structure, the anchorage of the columns longitudinal bars had a proper design, which prevented bond failure. In addition, the maximum damage of the center column occurs in a few cycles, which partially limits the effect of cyclic loads on bond degradation. Outside of considering the effect of slip, the steel reinforcement of the column ends in the anchorage areas was modeled, as shown in Fig. 7b, allowing a gradual transfer of stress from the longitudinal bars to concrete in this area.

The solid finite element models can lead to major convergence problems when they are used to represent the highly nonlinear behavior of concrete within an implicit time integration scheme [42,43]. In analysis where the structural elements remain in elastic range or suffer slight damages, implicit schemes are more efficient than explicit schemes because they require a smaller number of time steps to find the solution. However, when there is a significant damage and degradation in concrete members, time steps in an implicit scheme become too small to find equilibrium and achieve convergence, and sometimes they cannot be achieved. This convergence problem is a consequence of ill-conditioned matrices caused by material softening [44,45] and due to this explicit time integration schemes represent a viable option. The time step in this scheme is limited by the minimum size of the element mesh and the speed of sound propagation in the defined material. Although explicit time integration requires smaller time steps, convergence problems are much smaller and the time spent in solving the problem is relatively smaller because it is not necessary to invert matrices.

A material with bilinear plasticity and kinematic hardening was used for modeling the steel. In order to simplify the numerical model and reduce its computational cost, two material models were used to represent the behavior of the concrete. These two material models were used in zones that were defined according to the level of damage observed experimentally, and subsequently different levels of refinement in the finite element mesh were adopted for each zone. A linear elastic material was defined in the structural elements where no damage took place during the experimental tests. Since structural damage was concentrated in columns, the material model developed by Broadhouse and Neilson [46–48], called Winfrith Concrete Model, was used to represent its behavior. This material model was developed with the aim of predicting the response of reinforced concrete structures of the nuclear industry against impact loads, and has been used by several authors to simulate the behavior of concrete against impacts and blast loads [30,49–51]. The model uses a smeared

crack approach, with the possibility of taking into account variations in material properties as function of strain rate. The triaxial stress state in concrete is calculated from the composition of hydrostatic and deviatoric stresses. The hydrostatic stress is obtained from a volume compaction curve in function of the volumetric deformations. Furthermore, the deviatoric stress is linearly increased with strains increments until a yield surface based on criteria defined by Ottosen [2] is reached. This failure surface depends on three invariants from main and deviatoric stress tensors, and the surface shape is defined by four parameters.

The yield surface (F) is defined by the following expression:

$$F(I_1, J_2, \cos 3\theta) = a \cdot \frac{J_2}{f_c'^2} + \lambda \cdot \frac{\sqrt{J_2}}{f_c'} + b\frac{I_1}{f_c'} - 1 \quad (1)$$

where I_1 is the first invariant of the main stress tensor, J_2 is the second invariant of the deviatoric stress tensor, f'_c is the characteristic strength of concrete to uniaxial compression, a and b are parameters that define the meridional yield surface shape, and λ is a function of Lode angle θ defined by the following expression:

$$\lambda(\cos 3\theta) = \begin{cases} k_1 \cdot \cos\left[\frac{1}{3}\arccos(k_2 \cdot \cos 3\theta)\right] \text{ for } \cos 3\theta \geqslant 0 \\ k_1 \cdot \cos\left[\frac{\pi}{3} - \frac{1}{3}\arccos(-k_2 \cdot \cos 3\theta)\right] \text{ for } \cos 3\theta \leqslant 0 \end{cases} \quad (2)$$

where k_1 and k_2 are parameters that define the shape of the yield surface in the deviatoric plane. In the application of the yield surface to the Winfrith Concrete Model, the four parameters (a, b, k_1 and k_2) were defined as function of the relationship between tensile and compressive uniaxial strength of concrete [48]. The yield surface, when the tensile and compressive strength are defined with values according to Table 1, can be seen in Fig. 4.

When the stress reaches the failure surface, the flow stress is determined by a radial return algorithm, indicating a tensile failure when the maximum principal stress exceeds the tensile strength defined in the material properties. Once this takes place, the crack is marked in the plane perpendicular to maximum principal stress, allowing the model crack formation in up to three orthogonal planes. After the start of the crack, the tensile stress decreases linearly as function of the open width of the crack, and it becomes zero when a limit value of crack opening defined by the user is reached. As the deformation normal to crack increases, reduction also occurs in the shear stress that the element is capable of transferring trough the crack plane.

In real structures, large stiffness degradation may produce large localized strains with concrete cracking and crushing, and even separation or spalling of relatively large pieces of concrete from structural elements. In the numerical models, these large deformations may lead to serious distortions in the finite element mesh, causing blocking problems and a significant reduction of the time step size. Finite element programs with an explicit time integration scheme can reduce the effect of this problem by incorporating an erosion algorithm. Through this numerical tool, elements that reach a limit, set by some stress or strain criterion, are removed from the mesh of the numerical model. The LS-DYNA software has several erosion criteria, among which the criterion of the maximum effective strain and the maximum principal strain were selected because they have been successfully used in many previous studies [52–54]. The strain limit adopted in these previous studies has shown a great dispersion [55], and it has been proven that this limits depends on the mesh size and the type of loads to be represented [56]. For this reason it is necessary to calibrate the limit value of the erosion criterion and to compare the results with experimental results.

3.1. Mesh sensitivity analysis

In order to define the size of the finite element mesh of the numerical model that represents RC columns, a series of nonlinear dynamic analysis was performed. In all cases 10 cm elements were used in foundations of the structure and beams. In columns, three different element sizes (6.4 cm, 3.2 cm and 1.6 cm) were evaluated, as can be seen in Fig. 5. In order to ensure displacement compatibility between the parts with different element size, contact surfaces with kinematic constraint called "Tied Surface to Surface" [57] were used. The nodes on the interface, belonging to the finer mesh, were defined as slave nodes, and by the contact algorithm this nodes are forced to move along with the nodes of the coarser mesh, that were defined as master nodes. In this analysis, acceleration records measured on the shaking table in the first 24 s of the experimental test was used as load. The parameters of the concrete and steel material models were defined from the results of material test, as described later in Section 4. Since this mesh sensitivity analysis was performed prior to the analysis from which the parameters were calibrated, no erosion algorithm was implemented in this analysis and strain softening was not taken into account, assigning zero value to the crack width limit. This parameter and the erosion strain limit were calibrated, as detailed in Section 4, after defining the mesh size with the results of this study.

The dynamic responses, in terms of the displacement at the upper end of the center column and base shear of the same column, obtained from the numerical models with the different element sizes were compared to analyze the convergence of the results. These results are summarized in Fig. 6, where it can be seen the ratio between the results of the different models, in terms of displacement (Δ) and base shear (V), and the numerical results obtained from the model with the finest mesh (Δ_f and V_f). In this

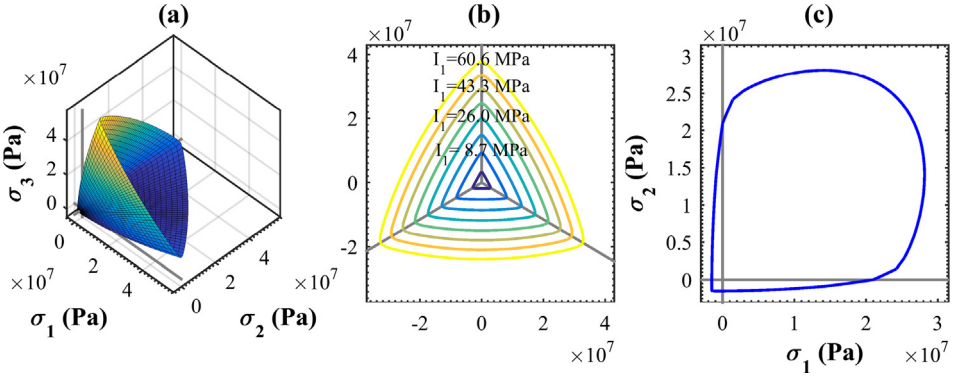

Fig. 4. Yield surface of concrete material model, a) main stress space, b) deviatoric plane, c) biaxial plane.

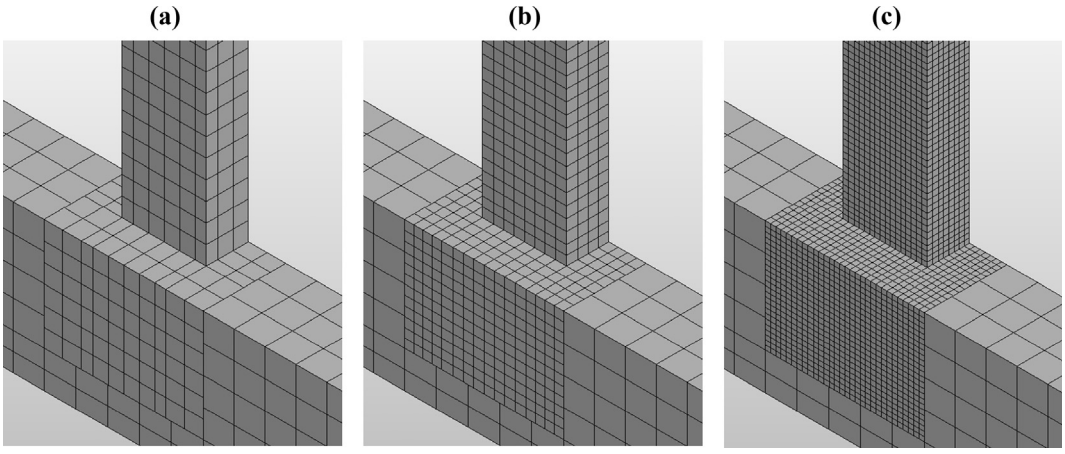

Fig. 5. Finite element mesh with different element sizes: a) 6.4 cm, b) 3.2 cm, c) 1.6 cm.

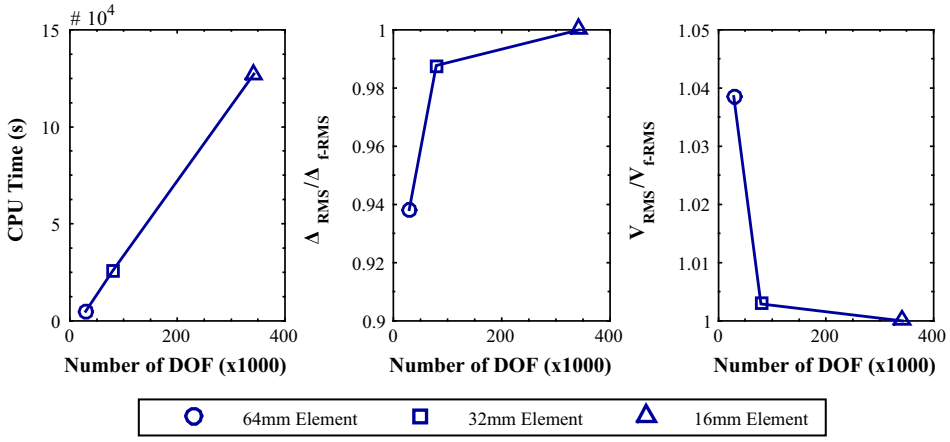

Fig. 6. Results of the mesh sensitivity analysis.

figure, it can also be seen the computational time spent on each case. In the case of the numerical model, where an element size of 3.2 cm was defined, the dynamic response presents differences smaller than 1.5% compared to the model where an element size of 1.6 cm was used, and requires 80% less time to complete the analysis. Thus, the element size of 3.2 cm was selected in the mesh of the numerical models used in subsequent sections, as can be seen in Fig. 7. A modal analysis was performed on the numerical model with the selected element size and a fundamental period of 0.227 s was obtained, which represents a relative difference of 3.18% with respect to that measured in experimental free vibration tests.

4. Calibration of material model parameters

The parameters that define the behavior of the steel material model are elastic modulus, yield stress, hardening modulus and ultimate strain. The values of these parameters were adopted according to the results of the material tests summarized in Table 2. Meanwhile, the behavior of the material model that represents concrete is defined by tension and compression strengths, elastic modulus, aggregate size and crack opening width from which normal and tangential stresses decrease to zero after tensile failure. Tension and compression strengths were established according to the results presented in Table 1. Since the material model remains linearly elastic until yield surface is reached, elastic modulus was defined as the secant modulus obtained from the ratio between the compressive strength and the strain measured when compressive stress attains its maximum value. An aggregate size of 9.53 mm was defined according to concrete mix specifications detailed in [1]. The parameters that remain undefined are the crack opening width, which is related to the strain softening in concrete, and the strain limit of the erosion algorithm, which allows to represent the higher degradation in concrete and to maintain numerical stability. In order to calibrate the crack width limit first, and subsequently calibrate the erosion strain limit, the sensitivity of the numerical response to the variation of these parameters was analyzed. Three similarity measures were established in order to quantify the agreement between the experimental response and the response of the different numerical models generated by assigning a discrete range of values to the parameters under study. These parameters were then calibrated by identifying the values that produce the highest correlation with the experimental response.

4.1. Crack width parameter calibration

The crack opening width, for which the element is no longer able to transmit forces in both tension and shear, was calibrated in first instance. For this calibration, the dynamic response of 5 models with different values assigned to the studied parameter was compared (0.02 mm, 0.05 mm, 0.10 mm, 0.15 mm and

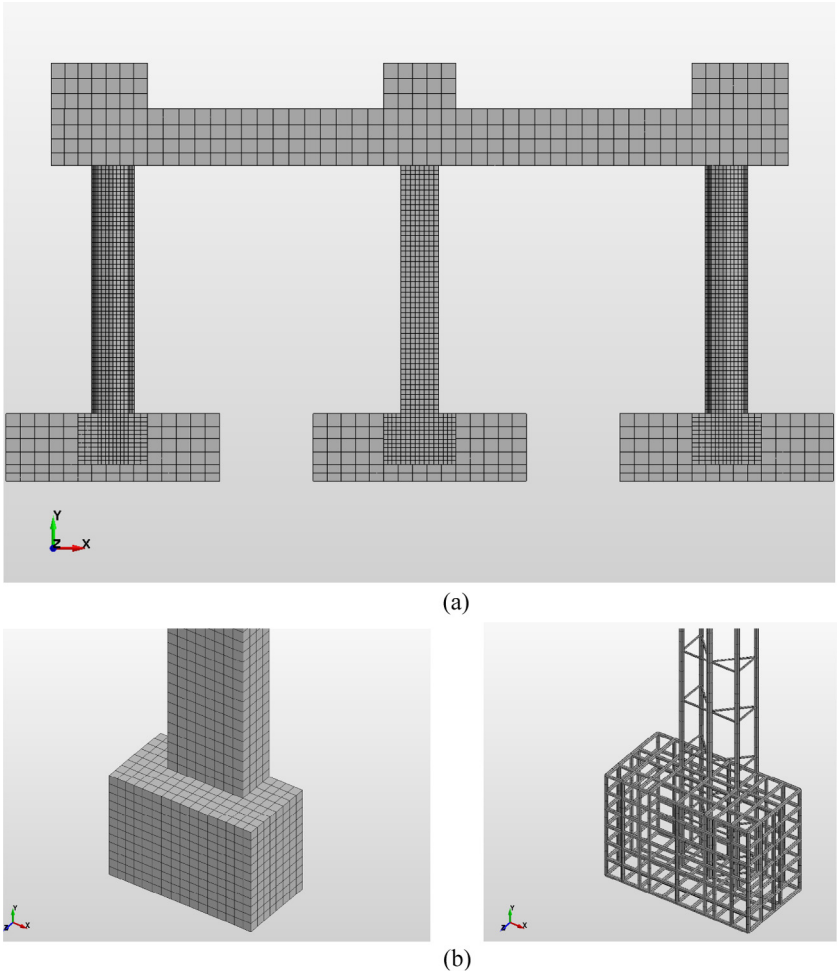

Fig. 7. Numerical model. a) Complete frame model. b) Detail of the center column.

0.20 mm). In order to establish the similarity degree between the experimental and numerical response, three indicators were used. The first is the normalized cross-correlation coefficient, which is defined according to the following expression:

$$R = \frac{\sum_i r_{\exp}[t_i] \cdot r_{num}[t_i]}{\sqrt{\sum_i r_{\exp}[t_i]^2 \cdot \sum_i r_{num}[t_i]^2}} \tag{3}$$

where R is the normalized cross-correlation coefficient, $r_{exp}[t_i]$ is the response recorded in the experimental test at time t_i and $r_{num}[t_i]$ is the response of the numerical model at the same time. This similarity measure is equal to 0 when there is no degree of similarity between the two signals, and is equal to 1 when the signals are exactly the same. However, the normalized cross-correlation coefficient is not sensitive to amplitude differences that may exist between the two signals compared. Therefore, the root mean square (RMS) value and the peak value, which themselves are indicators of the amplitude similarity of the signals, were also used as comparison criteria.

The material model parameter calibrated in this section allows reproducing the concrete damage that occurs prior to their total degradation. Meanwhile, the total degradation of the concrete is reproduced by material erosion, which was calibrated later and was not implemented in the numerical model used in the calibration of the crack width parameter. Due to this, the experimental response measured during the first 24 s of the experimental test was used as a reference for calibration, since after this time the major degradation was observed in the structure.

Fig. 8 shows the numerical response, in terms of displacements in the upper end of center column relative to foundation, obtained with the higher and lower value assigned to the parameter in this calibration. From this figure it can be seen how the frequency content of the response is modified in the different cases. This is because the model with different parameter values reaches different levels of damage, being this level of damage related to the value defined for the parameter under study. As can be seen in the figure, the lowest values of crack width caused the greatest amplitude of displacement and fewer cycles of oscillation, product of the sudden decrease in tensile stress

In Fig. 9, the values of similarity measures obtained in each case can be observed. The similarity measures, in terms of RMS and peak values, are expressed as a ratio of the displacement obtained from the numerical models (Δ_{num}) to the displacement measured experimentally (Δ_{exp}). The parameter value that resulted in the highest degree of similarity is highlighted in the figure. In this case, this value corresponds to a crack width limit of 0.02 mm according to the three indicators used. This figure also shows that the model response in terms of displacement is sensitive to the variation of the parameter analyzed.

Comparison of the different responses in terms of base shear in the center column is shown in Fig. 10. As was observed in the

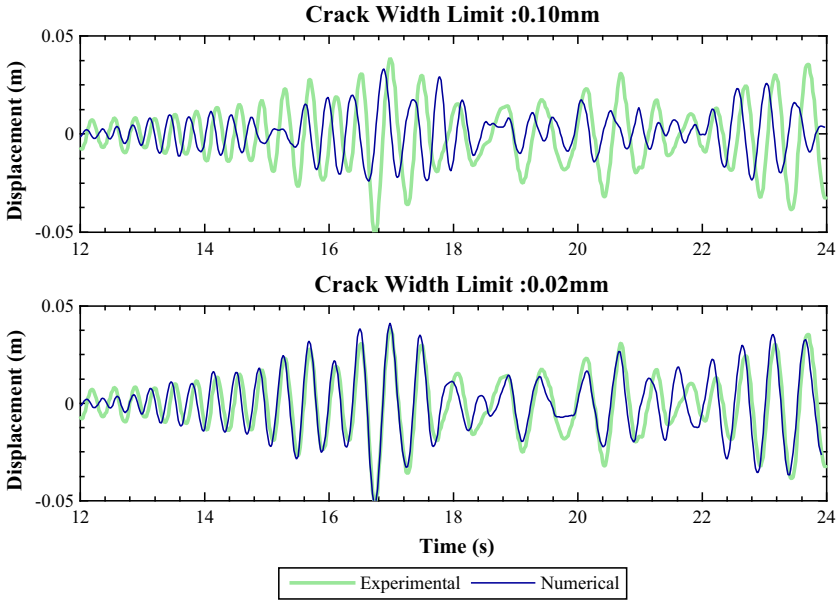

Fig. 8. Time history numerical-experimental displacement comparison.

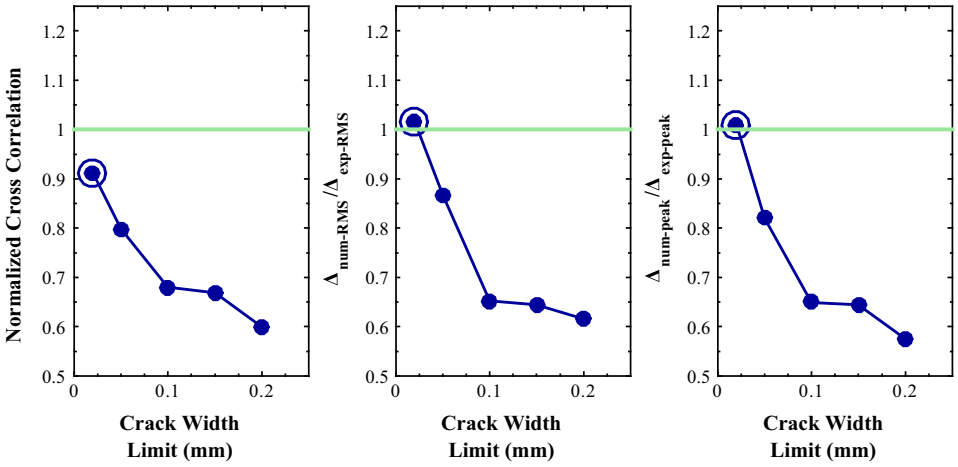

Fig. 9. Similarity measures of displacement comparison.

displacement comparison, the frequency content of the numerical response in terms of base shear also proved to be dependent on the crack width limit adopted. Furthermore, the response amplitude in this case was less sensitive to the variation of the studied parameter, with a slight increase in base shear as the crack width limit is increased. These observations are confirmed in Fig. 11, where the similarity degree achieved is shown in terms of normalized cross correlation and the ratio of numerical (V_{num}) to experimental (V_{exp}) base shear. In this figure the parameter value adopted as valid is also highlighted, and is coincident with the parameter value that produced the highest correlation of the numerical model in terms of displacements.

From the obtained results, it can be seen how a crack width limit of 0.02 mm provides the best correlation to the experimental response, both in terms of displacements and base shear. Adopting this value for the parameter studied, relative differences less than 2.5% in terms of RMS values and 4.3% in terms of peak values were obtained with a normalized cross-correlation coefficient greater than 0.91.

4.2. Erosion parameter calibration

Two strain based erosion criteria were compared in this calibration process. The first criterion states that the element is removed from the numerical model if the effective strain exceeds a defined limit value. This effective strain is obtained through the following expression:

$$\varepsilon_{eff} = \sqrt{\frac{2}{3} \cdot \varepsilon_{ij}^{dev} \cdot \varepsilon_{ij}^{dev}} \tag{4}$$

where ε_{eff} is the effective strain and ε_{ij}^{dev} are the components of the deviatoric strain tensor. The second erosion criterion analyzed uses the maximum principal strain to delete elements from the numerical model. This deformation is obtained as the maximum eigenvalue of the strain tensor. Models with 5 different strain limits (0.02 0.03, 0.04, 0.05 and 0.06) values were analyzed with each erosion criterion. In the numerical model the crack width parameter was adopted according to the calibration presented in the previous

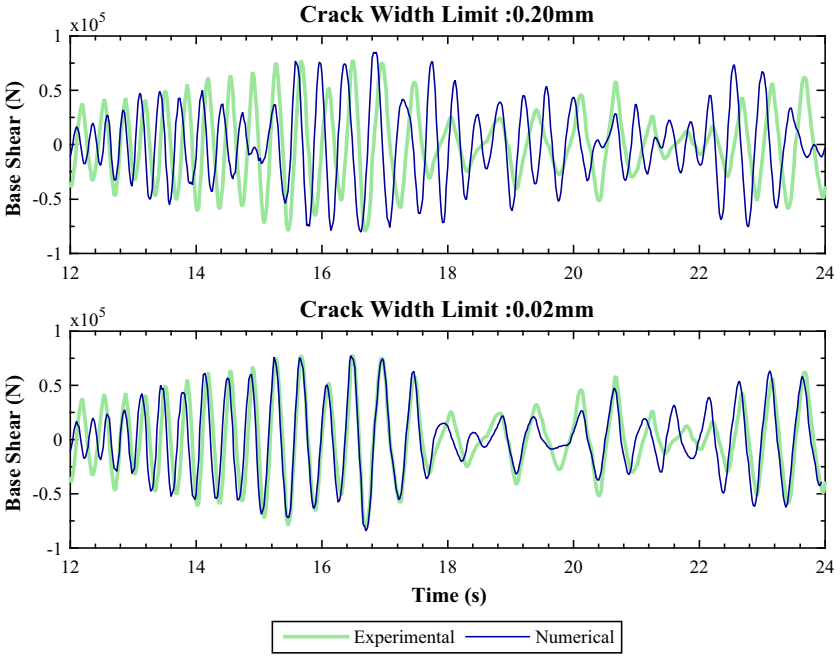

Fig. 10. Time history numerical-experimental base shear comparison.

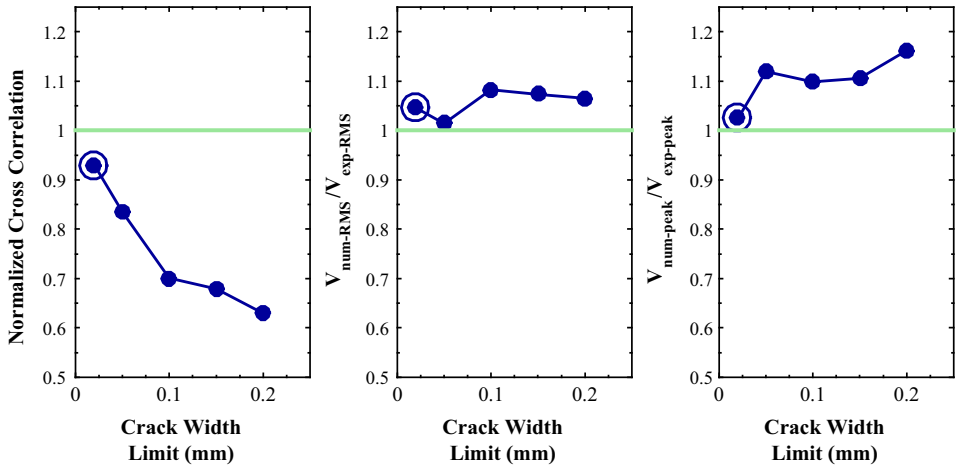

Fig. 11. Similarity measures of base shear comparison.

section. Unlike the previous calibration study, experimental numerical comparison was made with the first 30 s of the forced vibration test. This duration was selected because after 30 s the center column virtually ceases transferring shear forces to the base.

Fig. 12 shows the results obtained in terms of displacement when the numerical models are defined with the extreme parameter used in the present calibration. From these results it can be observed that for high values of the erosion limit, displacements and concrete degradation in the numerical model are lower than those observed experimentally. On the opposite, a higher concrete degradation can be observed in the numerical model when relatively low erosion limits are defined. In contrast to observations made in the calibration of crack width parameter, the model response during the initial 24 s is not substantially modified by the variation in the erosion criterion or strain limit imposed. This is because seismic action causes, in this initial part of the record, demands on the structure deformed below the limit of erosion, so the algorithm does not eliminate elements from the numerical model.

The degree of experimental numerical correlation achieved is presented in Fig. 13 as a function of different erosion criteria and limits evaluated. In this figure it can also be seen the relative difference between the displacements obtained from the different numerical models (Δ_{num}) and the displacements of the experimental model (Δ_{exp}). Previous observations on the sensitivity of the response in terms of displacements are confirmed in this figure, and it can be seen how the strain limit that produces the higher similarity measures is different for each erosion criterion. For effective strain criterion this strain limit value is 3%, while for the primary end deformation is 4%. Despite this fact, there were no major differences in the degree of similarity achieved by models with both erosion criteria when comparing with the experimental response.

Similar to the results obtained in terms of displacement, numerical-experimental comparison of base shear in center column for the different models analyzed are shown in Fig. 14. In contrast to the results observed in crack width calibration, in this case

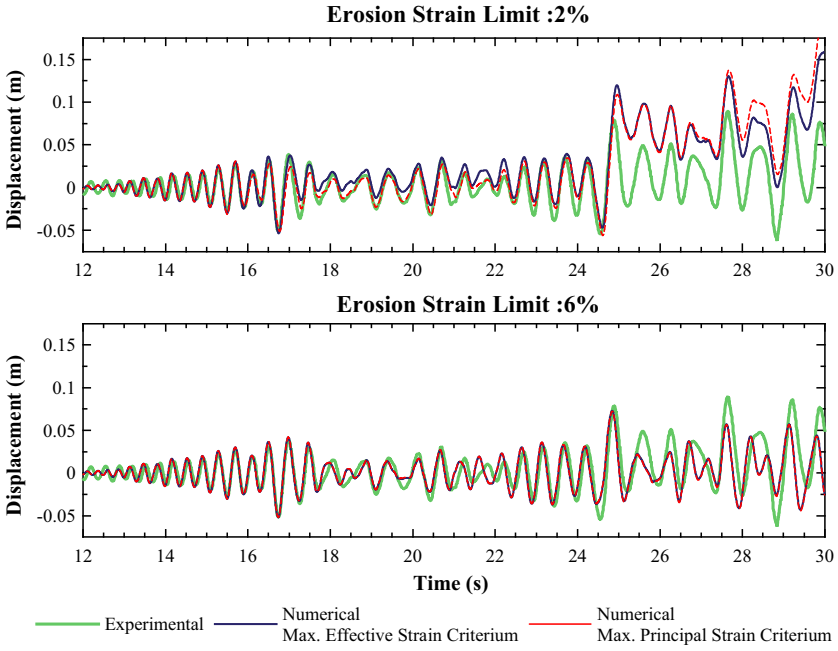

Fig. 12. Time history numerical-experimental displacement comparison.

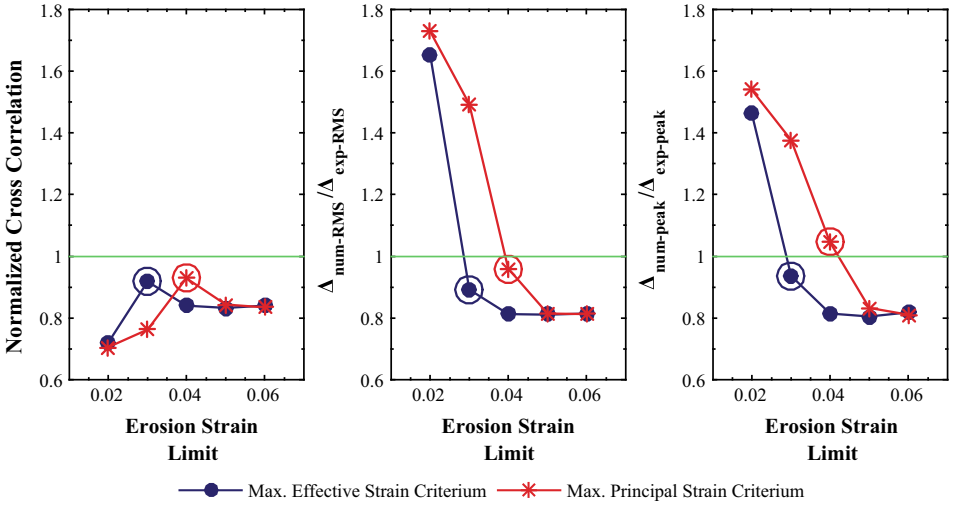

Fig. 13. Similarity measures of displacement comparison.

the variation of the parameter under study modifies significantly the amplitude of the response in terms of base shear, the parameter showing a large influence on the strength degradation.

The correlation degree obtained in terms of base shear is shown in Fig. 15 for the different criteria and limit erosion defined in the numerical model, expressed once again as a ratio of the numerical response (V_{num}) to the base shear measured experimentally (V_{exp}). From these results, similar trends to those already mentioned for the displacements can be observed. Once more, strain limit values that produce the higher similarity between the numerical and experimental responses for both criteria agree with the limits values obtained by analyzing the results in terms of displacement.

The numerical modeling methodology adopted therefore shows an acceptable degree of correlation with experimental response. In both cases normalized cross-correlation factors over 0.92 were achieved and the relative differences between the experimental and numerical response was lower in terms of base shear, not exceeding 5%, while in the case of displacement did not exceed 11%.

5. Numerical-experimental comparison

The results of the numerical model obtained using the calibrated values of the parameters (i.e. crack width limit of 0.02 mm, erosion limit of 3% for the effective strain criterion and 4% for the maximum principal strain criterion) are presented in this section. The numerical-experimental comparison in the time domain is shown in Fig. 16. In addition to the results already mentioned in the previous section, this figure shows the total base shear, which is obtained as the sum of the base shear in each column. It can be observed that the relative displacements of the upper end of the center column and the base shear achieve a high degree of correlation with experimental response, which was quantified in the previous section. From the figure it can also be

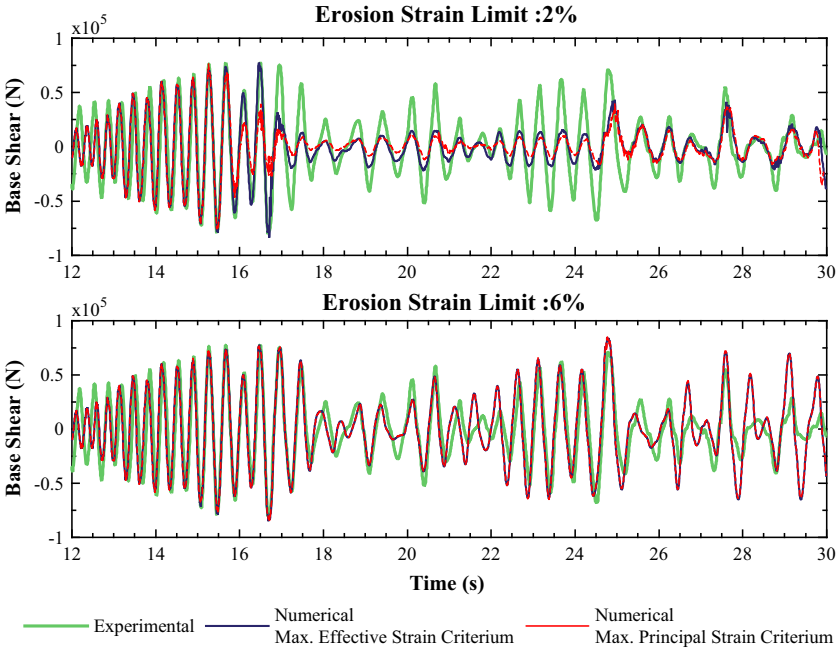

Fig. 14. Time history numerical-experimental base shear comparison.

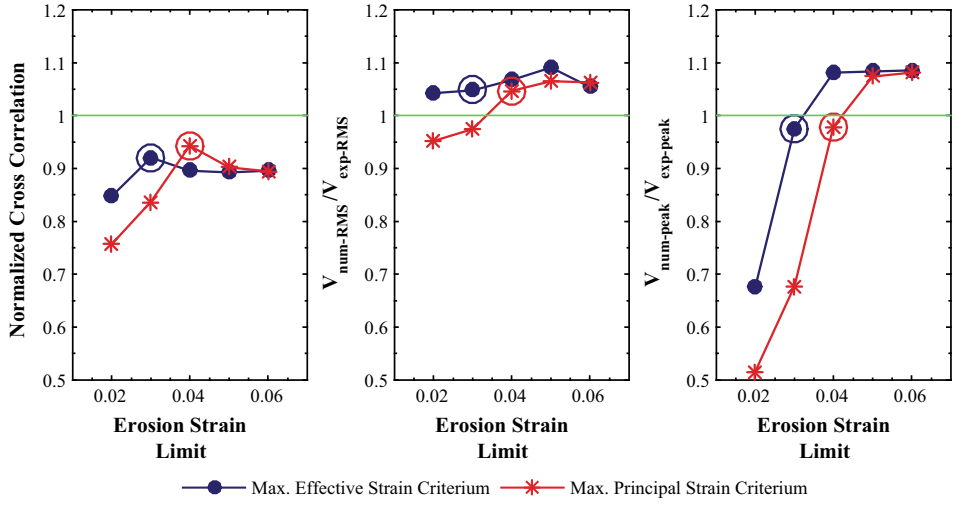

Fig. 15. Similarity measures of base shear comparison.

seen as the structural response amplitudes are well estimated by numerical models during the first 24 s, with a certain phase shift between 18 and 22 s. After the 24 s, some differences in amplitude can be observed, where relative displacements at the upper end of the center column and shear force at its base are underestimated. These differences can be attributed, among other effects, to the fact that the numerical model is not able to represent the cyclic effect of slip in the steel reinforcing bars, which causes a cumulative error that is more important once the maximum bond resistance is reached. Nevertheless, taking into account the highly nonlinear problem analyzed, a very good global agreement was obtained between numerical and experimental responses. In spite of this, and due to the complexity of the simulated behavior, it can be concluded that the model is able to acceptably reproduce the degradation in the RC column observed experimentally.

Fig. 17 shows the numerical-experimental comparison in the frequency domain. In general, the acceptable degree of correlation attained by the two numerical models is confirmed, with some differences in the maximum amplitudes of the displacements between 1 and 2 Hz. This difference results from the underestimation of the response by the numerical models after the 24 s. In terms of the base shear, it is possible to observe higher frequency content between 2 and 3 Hz compared to the response in terms of displacements. This is because the higher base shear occurred prior to the major damage of the center column, when the stiffness of the center column and the frequency of the response are higher.

The numerical-experimental comparison where the base shear of the center column is shown as function of the relative displacements of the upper end of the same column can be seen in Fig. 18. Similar observations to those made in the comparison of the two variables in time domain can be made in this case, observing a clear behavior in nonlinear range from 15 s and a noticeable stiffness and strength degradation from the 24 s of the seismic record. As mentioned before, and possibly due to the fact that the bar slip was not taken into account in the numerical

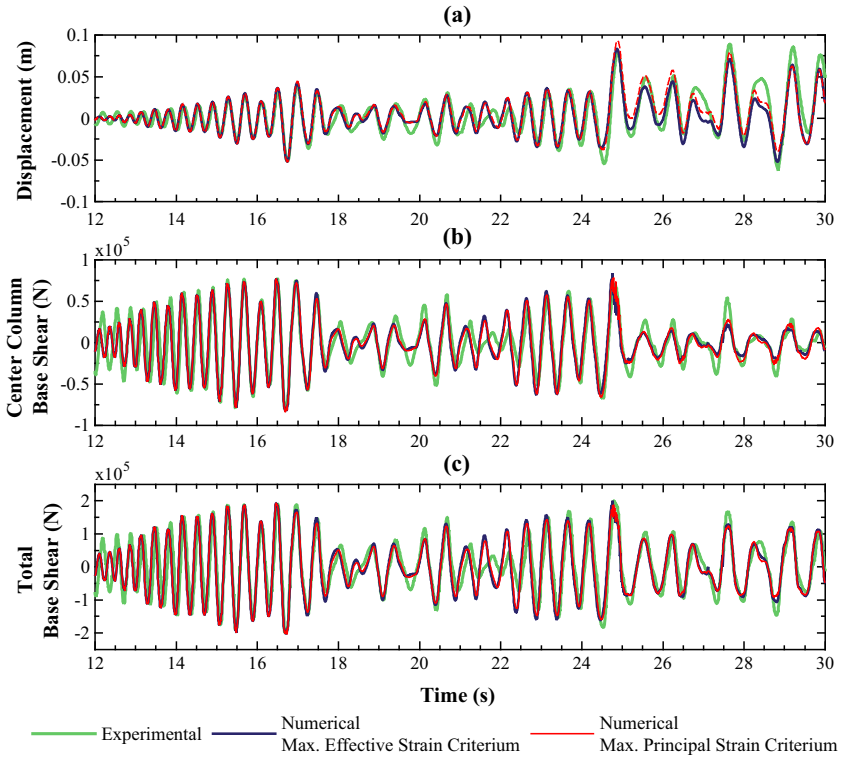

Fig. 16. Numerical-experimental comparison in time domain. a) Displacement of the upper end of center column relative to foundation, b) center column base shear, c) total base shear.

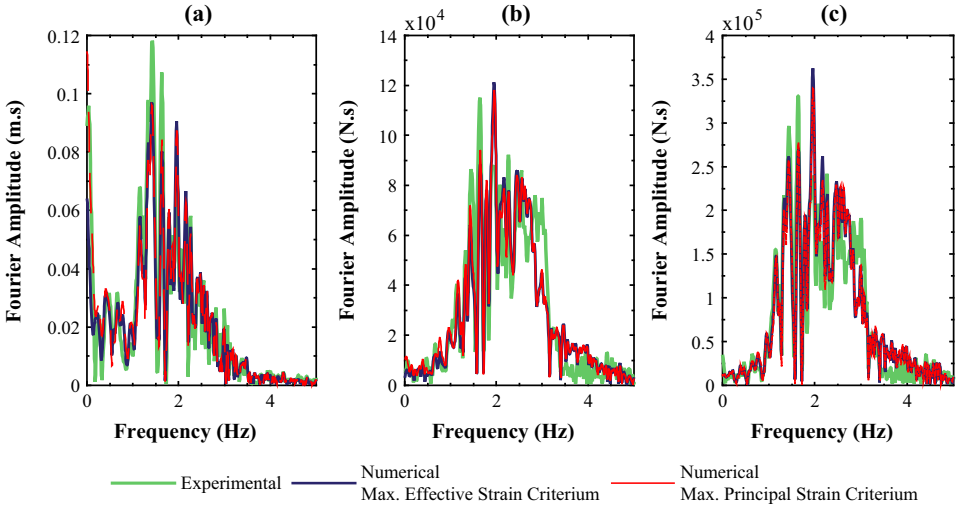

Fig. 17. Numerical-experimental comparison in frequency domain. a) Displacement of the upper end of center column relative to foundation, b) center column base shear, c) total base shear.

models, from this instant of time it can also be seen that both, displacement and base shear, amplitudes are underestimated. Despite this, the residual stiffness is shown to be similar to that observed experimentally.

The results are compared qualitatively in Figs. 19 and 20, where cracking patterns and the final configuration of the center column can be observed respectively. The cracking pattern of the upper end of the center column is shown in the instants when the clearly non-linear behavior starts (16.7 s) and when column degradation starts (24.9 s), observing similar cracks orientation in both cases on the numerical and experimental models. In the final configuration of center column, Fig. 20, a similar extent of the area where most concrete degradation was produced can be observed at the upper end of the column. At the lower end, it is seen as the erosion algorithm with principal strain criterion eliminated a greater number of elements that reached the limit strain established.

Considering the results presented in this section it can be concluded that a highly nonlinear dynamic response of RC frame under the effect of the seismic action can be numerically modeled with enough accuracy, both qualitatively and quantitatively, using the modeling approach described in this study.

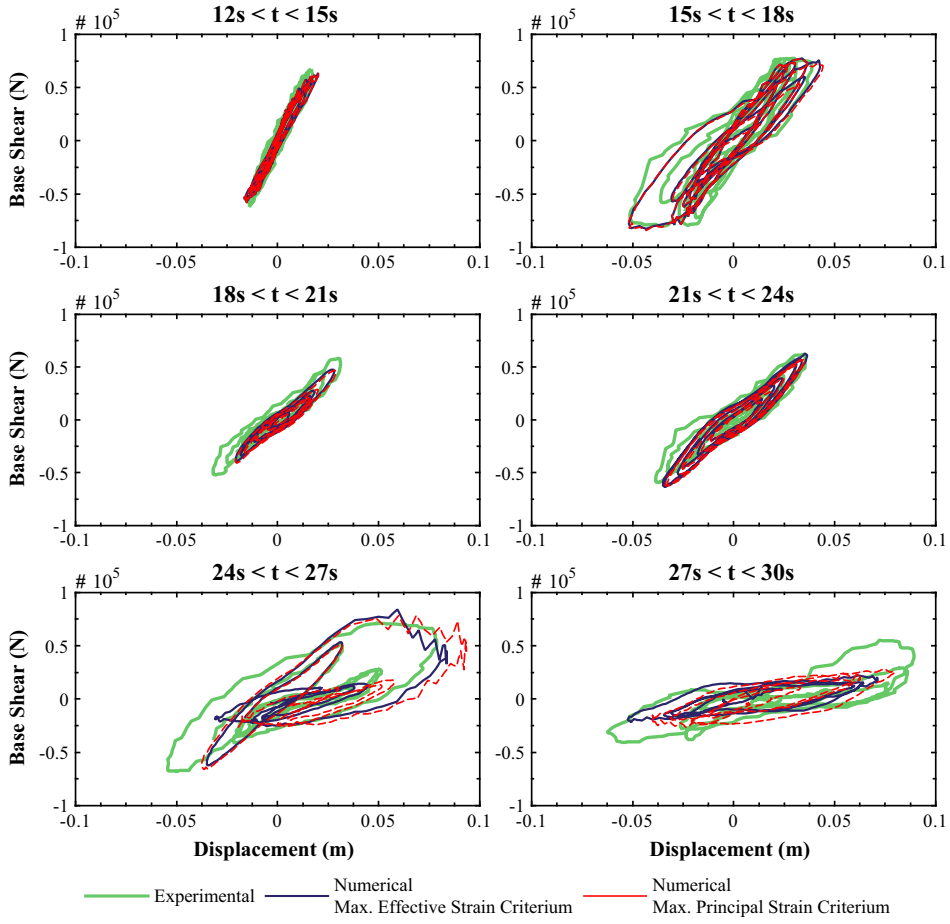

Fig. 18. Comparison of base shear as function of displacement.

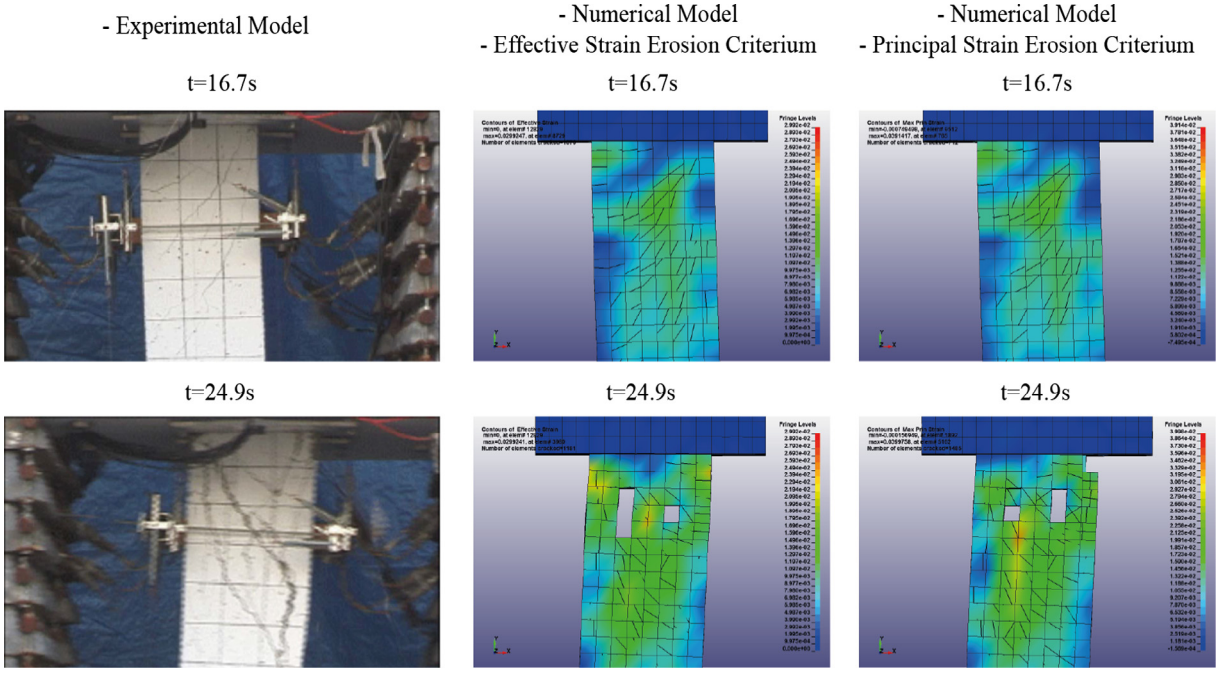

Fig. 19. Numerical-experimental comparison. Cracking pattern.

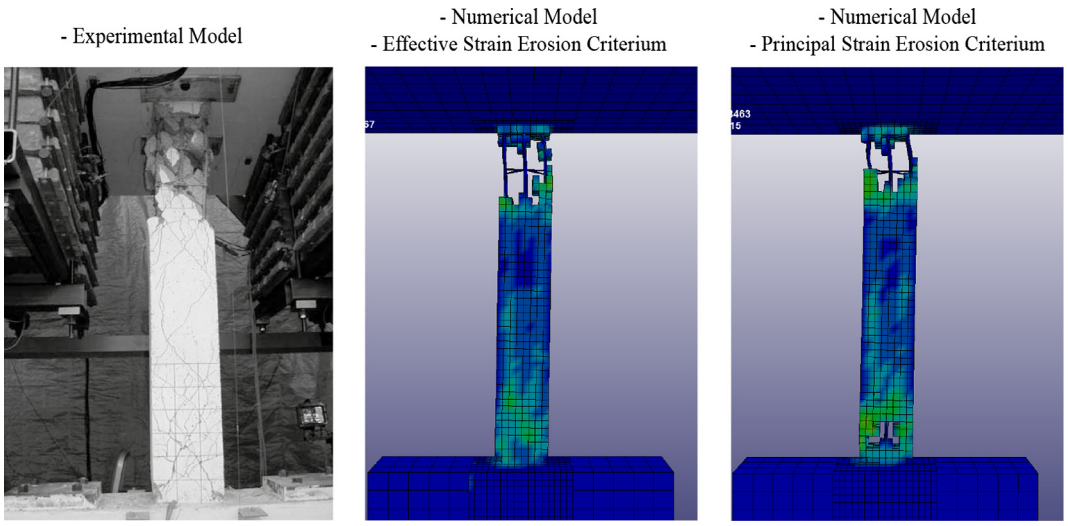

Fig. 20. Numerical-experimental comparison. Detail of the center column.

6. Conclusions

Throughout this work, the ability of the numerical modeling to represent a highly nonlinear dynamic response of RC frame under the effect of the seismic action was evaluated. The numerical model studied is composed of solid finite elements implemented within an explicit time integration scheme. This modeling approach was chosen because it is able to reproduce the nonlinear behavior of concrete structures in a general way, since a full three-dimensional stress state and the complete interaction between concrete and steel reinforcement can be directly represented. It should be mentioned that, although there are computationally less expensive methods, generally they cannot achieve convergence in analysis of RC members with high damage and degradation. Moreover, the continuous progress in computing power makes this kind of analysis more feasible within the research field of earthquake engineering. This technique has been previously used to represent the damage of reinforced concrete structures against blast and impact loads, but has been less commonly used for seismic actions. Because of this, a validation by comparison with experimental results, as that presented in this work, is necessary.

The experimental model response obtained from the shaking table tests documented by Elwood and Moehle [1], was used as reference. The numerical model was developed with LS-DYNA [23] software and the material model adopted uses the failure surface proposed by Ottosen [2] to represent the cracking and crushing of concrete. In the first instance, a mesh sensitivity analysis was performed, and subsequently the material model parameters were calibrated. The first parameter calibrated was the limit value of crack opening that makes normal tension stress decays to zero. In this calibration, the experimental response recorded previously to the highest damage in the structure was used as a reference. The response obtained from the numerical model was compared with the experimental response in terms of displacement and base shear. In order to establish the degree of agreement, three similarity measures were used: normalized cross correlation and relative differences between numerical and experimental response in RMS and peak values. Finally, the limit erosion value from which the elements are removed from the numerical model was calibrated. The experimental response that includes the greatest damage registered in the structure was used as reference in this case, having a high degradation of both stiffness and strength in the center column. The maximum effective strain and maximum principal strain erosion criteria were adopted.

The procedures and results obtained in this paper can serve as a modeling guide for the analysis of concrete structures that experience high degradation under the effect of the seismic action. The main guidelines and results can be summarized in the following conclusions:

- Solid finite elements with an explicit time integration scheme are suitable to reproduce the level of damage observed in the experimental RC structure, without the convergence problems that can be observed in implicit schemes [42–45].
- An element size of about 3 cm, which represents eight elements in the cross section, proved to be acceptable in terms of accuracy and computational cost.
- A crack opening width of 0.02 mm produced the highest numerical-experimental correlation. A normalized cross correlation greater than 0.91 was achieved and relative differences in RMS and peaks under 4.3% were observed.
- Limit strain values of 3% and 4% for the maximum effective strain and maximum principal strain erosion criteria respectively, produced the best agreement when compared with the experimental response. The achieved similarity indices were similar for the two erosion criteria, both in terms of displacement as base shear in the center column, with a normalized cross-correlation superior to 0.92 in all cases and relative differences lower than 11%.

Acknowledgements

The financial support of CONICET and the National University of Cuyo is gratefully acknowledged. Special acknowledgements are extended to the reviewers of the first version of the paper because their useful suggestions led to improvements of the work.

References

[1] Elwood K, Moehle J. Shake table tests and analytical studies on the gravity load collapse of reinforced concrete frames, Rep. 2003/01. Berkeley, Calif.: Pacific Earthquake Engineering Research Center, Univ. of California; 2003.
[2] Ottosen NS. A failure criterion for concrete. J Eng Mech 1977;527–535.
[3] Shayanfar J, Akbarzadeh Bengar H, Niroomandi A. A proposed model for predicting nonlinear behavior of RC joints under seismic loads. Mater Des 2016;95:563–79. http://dx.doi.org/10.1016/j.matdes.2016.01.098.
[4] López-López A, Tomás A, Sánchez-Olivares G. Influence of adjusted models of plastic hinges in nonlinear behaviour of reinforced concrete buildings. Eng Struct 2016;124:245–57. http://dx.doi.org/10.1016/j.engstruct.2016.06.021.

[5] Lepage A, Hopper MW, Delgado SA, Dragovich JJ. Best-fit models for nonlinear seismic response of reinforced concrete frames. Eng Struct 2010;32:2931–9. http://dx.doi.org/10.1016/j.engstruct.2010.05.012.
[6] Babazadeh A, Burgueño R, Silva PF. Evaluation of the critical plastic region length in slender reinforced concrete bridge columns. Eng Struct 2016;125:280–93. http://dx.doi.org/10.1016/j.engstruct.2016.07.021.
[7] Borghini A, Gusella F, Vignoli A. Seismic vulnerability of existing R.C. buildings: a simplified numerical model to analyse the influence of the beam-column joints collapse. Eng Struct 2016;121:19–29. http://dx.doi.org/10.1016/j.engstruct.2016.04.045.
[8] Hatzigeorgiou GD, Liolios AA. Nonlinear behaviour of RC frames under repeated strong ground motions. Soil Dyn Earthquake Eng 2010;30:1010–25. http://dx.doi.org/10.1016/j.soildyn.2010.04.013.
[9] Xu S-Y, Zhang J. Axial–shear–flexure interaction hysteretic model for RC columns under combined actions. Eng Struct 2012;34:548–63. http://dx.doi.org/10.1016/j.engstruct.2011.10.023.
[10] Birely AC, Lowes LN, Lehman DE. A model for the practical nonlinear analysis of reinforced-concrete frames including joint flexibility. Eng Struct 2012;34:455–65. http://dx.doi.org/10.1016/j.engstruct.2011.09.003.
[11] Spacone E, Filippou FC, Taucer FF. FIBRE beam-column model for non-linear analysis of R/C frames: Part I. Formulation. Earthquake Eng Struct Dyn 1996;25:711–25. http://dx.doi.org/10.1002/(SICI)1096-9845(199607)25:7∗711::AID-EQE576∗3.0.CO;2-9.
[12] Spacone E, Filippou FC, Taucer FF. FIBRE beam-column model for non-linear analysis of R/C frames: Part II. Applications. Earthquake Eng Struct Dyn 1996;25:727–42. http://dx.doi.org/10.1002/(SICI)1096-9845(199607)25:7∗727::AID-EQE577∗3.0.CO;2-O.
[13] Arshian AH, Morgenthal G, Narayanan S. Influence of modelling strategies on uncertainty propagation in the alternate path mechanism of reinforced concrete framed structures. Eng Struct 2016;110:36–47. http://dx.doi.org/10.1016/j.engstruct.2015.11.019.
[14] Kashani MM, Lowes LN, Crewe AJ, Alexander NA. Nonlinear fibre element modelling of RC bridge piers considering inelastic buckling of reinforcement. Eng Struct 2016;116:163–77. http://dx.doi.org/10.1016/j.engstruct.2016.02.051.
[15] Li Z-X, Gao Y, Zhao Q. A 3D flexure–shear fiber element for modeling the seismic behavior of reinforced concrete columns. Eng Struct 2016;117:372–83. http://dx.doi.org/10.1016/j.engstruct.2016.02.054.
[16] Li Z, Hatzigeorgiou GD. Seismic damage analysis of RC structures using fiber beam-column elements. Soil Dyn Earthquake Eng 2012;32:103–10. http://dx.doi.org/10.1016/j.soildyn.2011.09.001.
[17] Nguyen XH. Performance of multifiber beam element for seismic analysis of reinforced concrete structures. Int J Struct Stab Dyn 2014;14:1450013. http://dx.doi.org/10.1142/S0219455414500138.
[18] Ravi Mullapudi T, Ayoub A. Modeling of the seismic behavior of shear-critical reinforced concrete columns. Eng Struct 2010;32:3601–15. http://dx.doi.org/10.1016/j.engstruct.2010.08.004.
[19] Martinelli L, Martinelli P, Mulas MG. Performance of fiber beam–column elements in the seismic analysis of a lightly reinforced shear wall. Eng Struct 2013;49:345–59. http://dx.doi.org/10.1016/j.engstruct.2012.11.010.
[20] Silva Lobo P, Almeida J. RC fiber beam–column model with bond-slip in the vicinity of interior joints. Eng Struct 2015;96:78–87. http://dx.doi.org/10.1016/j.engstruct.2015.04.005.
[21] LeBorgne MR, Ghannoum WM. Calibrated analytical element for lateral-strength degradation of reinforced concrete columns. Eng Struct 2014;81:35–48. http://dx.doi.org/10.1016/j.engstruct.2014.09.030.
[22] Caprili S, Nardini L, Salvatore W. Evaluation of seismic vulnerability of a complex RC existing building by linear and nonlinear modeling approaches. Bull Earthquake Eng 2012;10:913–54. http://dx.doi.org/10.1007/s10518-011-9329-4.
[23] J.O. Hallquist, LS-DYNA theory manual, 2006.
[24] Chen W, Hao H, Chen S. Numerical analysis of prestressed reinforced concrete beam subjected to blast loading. Mater Des 2015;65:662–74. http://dx.doi.org/10.1016/j.matdes.2014.09.033.
[25] Zhao CF, Chen JY, Wang Y, Lu SJ. Damage mechanism and response of reinforced concrete containment structure under internal blast loading. Theor Appl Fract Mech 2012;61:12–20. http://dx.doi.org/10.1016/j.tafmec.2012.08.002.
[26] Tai YS, Chu TL, Hu HT, Wu JY. Dynamic response of a reinforced concrete slab subjected to air blast load. Theor Appl Fract Mech 2011;56:140–7. http://dx.doi.org/10.1016/j.tafmec.2011.11.002.
[27] Bao X, Li B. Residual strength of blast damaged reinforced concrete columns. Int J Impact Eng 2010;37:295–308. http://dx.doi.org/10.1016/j.ijimpeng.2009.04.003.
[28] Yao S, Zhang D, Lu F, Wang W, Chen X. Damage features and dynamic response of RC beams under blast. Eng Fail Anal 2016;62:103–11. http://dx.doi.org/10.1016/j.engfailanal.2015.12.001.
[29] Thai D-K, Kim S-E. Failure analysis of reinforced concrete walls under impact loading using the finite element approach. Eng Fail Anal 2014;45:252–77. http://dx.doi.org/10.1016/j.engfailanal.2014.06.006.
[30] Sadiq M, Xiu Yun Z, Rong P. Simulation analysis of impact tests of steel plate reinforced concrete and reinforced concrete slabs against aircraft impact and its validation with experimental results. Nucl Eng Des 2014;273:653–67. http://dx.doi.org/10.1016/j.nucengdes.2014.03.031.
[31] Orbovic N, Sagals G, Blahoianu A. Influence of transverse reinforcement on perforation resistance of reinforced concrete slabs under hard missile impact. Nucl Eng Des 2015;295:716–29. http://dx.doi.org/10.1016/j.nucengdes.2015.06.007.
[32] Lee H-K, Kim S-E. Comparative assessment of impact resistance of SC and RC panels using finite element analysis. Prog Nucl Energy 2016;90:105–21. http://dx.doi.org/10.1016/j.pnucene.2016.03.002.
[33] Huang C-C, Wu T-Y. A study on dynamic impact of vertical concrete cask tip-over using explicit finite element analysis procedures. Ann Nucl Energy 2009;36:213–21. http://dx.doi.org/10.1016/j.anucene.2008.11.014.
[34] Elwood KJ, Moehle JP. Dynamic shear and axial-load failure of reinforced concrete columns. J Struct Eng 2008;134:1189–98. http://dx.doi.org/10.1061/(ASCE)0733-9445(2008)134:7(1189).
[35] Lynn AC. Seismic evaluation of existing reinforced concrete building columns. Berkeley: University of California; 2001.
[36] Sezen H. Seismic behavior and modeling of reinforced concrete building columns. Berkeley: University of California; 2002.
[37] Flanagan DP, Belytschko T. A uniform strain hexahedron and quadrilateral with orthogonal hourglass control. Int J Numer Methods Eng 1981;17:679–706. http://dx.doi.org/10.1002/nme.1620170504.
[38] Hughes TJR, Liu WK. Nonlinear finite element analysis of shells: Part I. Three-dimensional shells. Comput Methods Appl Mech Eng 1981;26:331–62. http://dx.doi.org/10.1016/0045-7825(81)90121-3.
[39] Hughes TJR, Liu WK. Nonlinear finite element analysis of shells-part II. Two-dimensional shells. Comput Methods Appl Mech Eng 1981;27:167–81. http://dx.doi.org/10.1016/0045-7825(81)90148-1.
[40] Eligehausen R, Popov EP, Bertero VV. Local bond stress-slip relationships of deformed bars under generalized excitations. California, USA: Berkeley; 1983.
[41] Pochanart S, Harmon T. Bond-slip model for generalized excitations including fatigue. ACI Mater J 1989;86:465–74. http://dx.doi.org/10.14359/2052.
[42] Kianoush MR, Acarcan M, Ziari A. Behavior of base restrained reinforced concrete walls under volumetric change. Eng Struct 2008;30:1526–34. http://dx.doi.org/10.1016/j.engstruct.2007.10.009.
[43] Oliver J, Linero DL, Huespe AE, Manzoli OL. Two-dimensional modeling of material failure in reinforced concrete by means of a continuum strong discontinuity approach. Comput Methods Appl Mech Eng 2008;197:332–48. http://dx.doi.org/10.1016/j.cma.2007.05.017.
[44] Dhanasekar M, Haider W. Explicit finite element analysis of lightly reinforced masonry shear walls. Comput Struct 2008;86:15–26. http://dx.doi.org/10.1016/j.compstruc.2007.06.006.
[45] Oliver J, Huespe AE, Blanco S, Linero DL. Stability and robustness issues in numerical modeling of material failure with the strong discontinuity approach. Comput Methods Appl Mech Eng 2006;195:7093–114. http://dx.doi.org/10.1016/j.cma.2005.04.018.
[46] B.J. Broadhouse, A.J. Neilson, Modelling Reinforced Concrete Structures in DYNA3D, Rep. AEEW-M2465, UK At. Energy Authority, Winfrith. (1987).
[47] B.J. Broadhouse, SPD/D(95)363. AEA Technology. Winfrith Concrete Model in LS-DYNA3D, 1995.
[48] Schwer L. An introduction to the Winfrith concrete model. Serv: Schwer Eng. Consult; 2010.
[49] Arros J, Doumbalski N. Analysis of aircraft impact to concrete structures. Nucl Eng Des 2007;237:1241–9. http://dx.doi.org/10.1016/j.nucengdes.2006.09.044.
[50] Epackachi S, Whittaker AS, Varma AH, Kurt EG. Finite element modeling of steel-plate concrete composite wall piers. Eng Struct 2015;100:369–84. http://dx.doi.org/10.1016/j.engstruct.2015.06.023.
[51] Thiagarajan G, Kadambi AV, Robert S, Johnson CF. Experimental and finite element analysis of doubly reinforced concrete slabs subjected to blast loads. Int J Impact Eng 2015;75:162–73. http://dx.doi.org/10.1016/j.ijimpeng.2014.07.018.
[52] Teng T-L, Chu Y-A, Chang F-A, Shen B-C, Cheng D-S. Development and validation of numerical model of steel fiber reinforced concrete for high-velocity impact. Comput Mater Sci 2008;42:90–9. http://dx.doi.org/10.1016/j.commatsci.2007.06.013.
[53] Nyström U, Gylltoft K. Numerical studies of the combined effects of blast and fragment loading. Int J Impact Eng 2009;36:995–1005. http://dx.doi.org/10.1016/j.ijimpeng.2009.02.008.
[54] Hao Y, Hao H, Li Z-X. Numerical analysis of lateral inertial confinement effects on impact test of concrete compressive material properties. Int J Prot Struct 2010;1:145–68. http://dx.doi.org/10.1260/2041-4196.1.1.145.
[55] Luccioni B, Araoz G. Erosion criteria for frictional materials under blast load. MEC Comput 2011:1809–31. www.amcaonlin.org.ar.
[56] Luccioni B, Aráoz G, Labanda N. Defining erosion limit for concrete. Int J Prot Struct 2013;4:315–40. http://dx.doi.org/10.1260/2041-4196.4.3.315.
[57] Bala S. Contact modeling in LS-DYNA-some recommendations – Part 1. FEA Inf Int News 2001;2:8–16.